Available online at www.sciencedirect.com
ScienceDirect
Tectonophysics 429 (2007) 165–181
TECTONOPHYSICS
www.elsevier.com/locate/tecto

Stress tensor and focal mechanisms along the Dead Sea fault and related structural elements based on seismological data

Rami Hofstetter [a,*], Yann Klinger [b,d], Abdel-Qader Amrat [c], Luis Rivera [b], Louis Dorbath [b]

[a] *Seismology Division, Geophysical Institute of Israel, Lod 71100, Israel*
[b] *UMR 7516, Institut de Physique du Globe, 5 rue René Descartes, 67084 Strasbourg, France*
[c] *Natural Resources Authority, Amman, Jordan*
[d] *UMR7154, boite 89, IPG Paris, 4, place Jussieu, 75005 Paris, France*

Received 27 July 2005; received in revised form 13 February 2006; accepted 22 March 2006
Available online 1 December 2006

Abstract

The Dead Sea fault is among the largest active strike–slip fault of the world. This study is focused on the southern part of this fault, from the Sea of Galilee to the Gulf of Aqaba, as monitored mainly by the Jordanian and Israeli seismic networks. The data of arrival times and polarities allowed relocation of earthquakes with a better azimuthal coverage and computation of focal mechanisms. This last step has been realized by inverting the polarities to determine a unique stress tensor for the region and the compatible focal mechanisms. Inversion with different subsets of the data set, based on tectonic regionalization, has also been performed to evaluate the impact of each cluster of earthquakes on the global solution. The population of focal mechanisms is clearly dominated by strike–slip events, with the notable exception of a cluster of earthquakes, south of the Dead Sea, which displays several normal focal mechanisms. This last cluster forces σ_1 to be vertical and σ_2 to be horizontal. A large number of fault planes, however, are close to the vertical, inhibiting the action of the vertical component of the stress tensor, and acting like under strike–slip stress regime. We observed a good agreement between the location of the earthquakes and the active faults, based on geological data. In addition, there is a good agreement between the fault plane solutions and the orientation of the active faults.

Keywords: Dead Sea fault; Focal mechanism; Stress tensor

1. Introduction

The Dead Sea fault (DSF) is one of the longest active strike–slip faults of the world. The DSF, about 1200 km long, connects the Taurus–Zagros compressional front, in the north, to the extensional zone of the Red Sea (Fig. 1). Quennell (1958) suggested 62 km of sinistral movement by the end of the first phase (pre-Neogene) and 45 km of movement in the second phase (possibly still continuing), which probably began in the Pleistocene. Further studies added important information on various parts of the fault and the mechanical behaviour (e.g., Freund et al., 1970; Bartov et al., 1980; Garfunkel, 1981; Kashai and Crocker, 1987; Barjous and Mikbel, 1990; Atallah, 1992; Sneh, 1996). Khair (2001) describes the geomorphology and seismicity of the Roum fault in Lebanon and its relation to the Dead Sea fault. In situ stress measurements and focal mechanisms solutions of three strong

* Corresponding author.
E-mail address: rami@seis.mni.gov.il (R. Hofstetter).

0040-1951/$ - see front matter © 2006 Elsevier B.V. All rights reserved.
doi:10.1016/j.tecto.2006.03.010

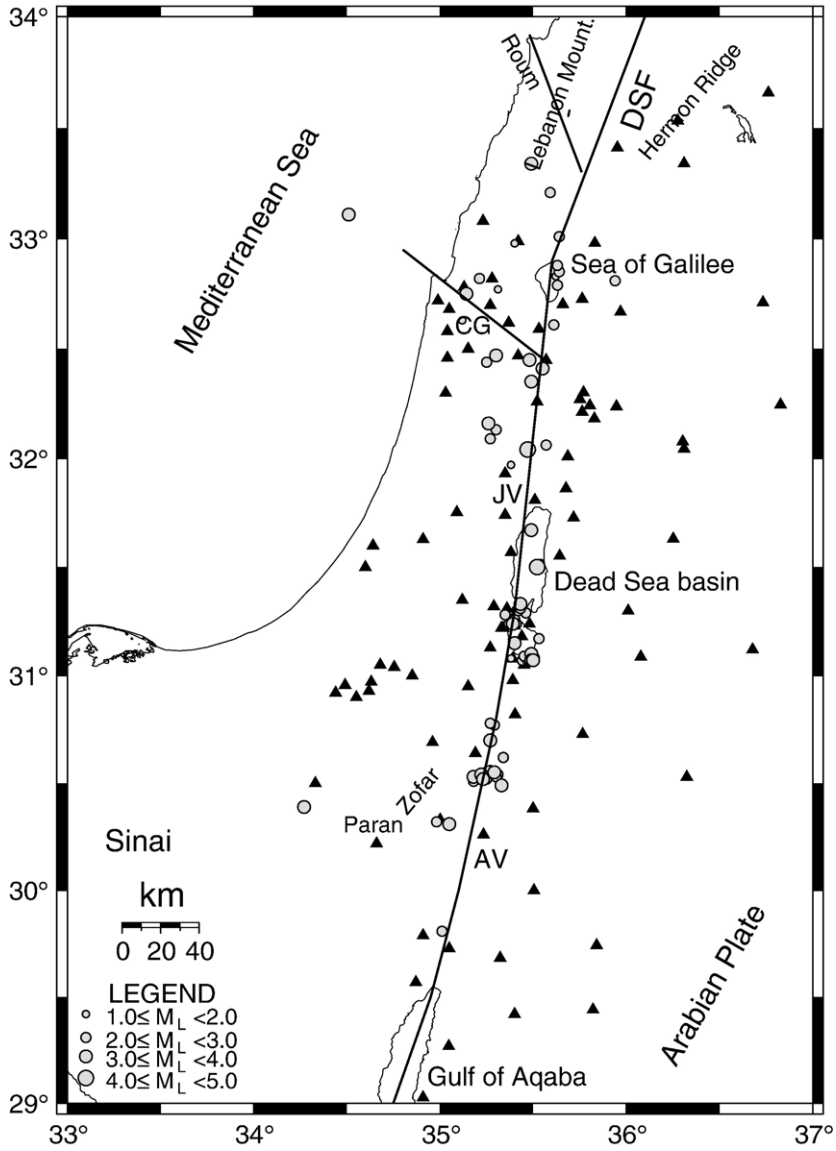

Fig. 1. The 78 earthquakes that have been relocated during the years 1987–1996 (open circles). The threshold magnitude is about M_L=2. Seismic stations used at least once in this study are presented by open triangles. The main active tectonic structures are figured by black lines.

earthquakes along the Dead Sea fault suggest a strike–slip regime with a remarkable thrust faulting component (Badawy and Horváth, 1999). Pe'eri et al. (2002) and Le Beon et al. (2006) reported that the relative plate motion across the Dead Sea fault is a few millimeters based on GPS continuous measurements during 5 years and in agreement with the seismological and geological observations. Aldersons et al. (2003) studied the local seismicity in the Dead Sea basin as related to thermomechanical model, suggesting that large portion of the earthquake nucleation occurred in the lower crust.

In this study we focus on the area located between the Sea of Galilee and the Gulf of Aqaba (Fig. 1). Our aim is to present new insights about the stress field acting in the area and to report on a newly acquired set of focal mechanisms for earthquakes that occurred during the period 1987–1996. Historical seismicity (i.e., Amiran et al., 1994) and instrumental seismicity observed in the early 20th century (i.e., Salamon et al., 1996) exhibit large mislocation errors. Most of those events are relatively large and are probably associated with the activity of the Dead Sea fault, and it is practically impossible to associate them with the small off-Dead-Sea faults.

Knowledge of the stress field in a region is an important tool to understand local and regional effects induced by large-scale plate tectonics and the subsequent deformation field. According to the objects used to retrieve the stress field, different time periods are sampled. On one hand, slikensides measured on a sedimentary or crystalline outcrop describe the whole tectonic history experienced by the region. On the other hand, seismological data give an instantaneous picture of the present-day stress field. For example, Lund and Slunga (1999) presented stress tensor inversion based on detailed microearthquake data in southwest Iceland. Together with accurate relative location, it was possible to assign a common fault plane to a cluster of events. Hauksson (1994) and Hardebeck and Hauksson (2001), based on inversion of earthquakes, presented a spatial heterogeneous image of stress orientation in southern California, as a result of the complexity of faulting. In this paper, the orientation and the shape of the stress tensor in Israel and Jordan are determined from the regional seismological data, providing us with the present-day state of stress prevailing in the region. Wherever possible, we compare our results with those obtained from recent geological observations.

2. Tectonic setting of the Dead Sea region

The Dead Sea fault is roughly linear (Fig. 1) at the exception of one major bend, responsible for the uplift of the Lebanon and Hermon ridges, north of the region under study. Several long individual segments that are connected through large extensional jogs, like the Dead Sea basin, form most of the fault (Garfunkel, 1981; Reches and Hoexter, 1981).

At the southern end of the DSF, the Gulf of Aqaba is formed by the series of three deep pull-apart (Ben-Avraham, 1985). It is surrounded by the Sinai Mountains to the west, which show large inherited systems of faults mostly oriented parallel to the gulf (Eyal et al., 1981) and Hejaz Mountains to the east showing a similar pattern. The strong earthquake that occurred in the Gulf of Aqaba in 1995 (Baer et al., 1999; Klinger et al., 1999, 2000a; Hofstetter et al., 2003) recalls that the DSF is still active.

From the Gulf of Aqaba to the Dead Sea basin, the DSF cross-cuts quaternary sediments of the Arava Valley (Wadi Araba). The fault is almost purely strike–slip in this section and is composed of linear segments several tens of kilometers long connected either by compressive or extensive jogs that form, respectively, small-scale push-ups or basins (Garfunkel, 1981; Reches and Hoexter, 1981; Ginat et al., 1998; Klinger et al., 2000b). Consequently, the topography associated with the active fault is low. The Arava Valley is flanked on both sides by large plateaus, which exhibit only recent small deformations. West of the Arava valley, however, some topographic heights intercept the Arava valley between 30°N and 31°N, related to the central Sinai shear zone (Bartov, 1974; Garfunkel, 1981; Powell and Khalil, 1993). It is highly probable that some of the structures still interact with the DSF at the junction of the two systems (Eyal, 1996; Frieslander et al., 1997; Frieslander, 2000).

The Dead Sea basin is the largest extensional step-over (100 km × 20 km) along the DSF. It connects the Wadi Araba–Dead Sea segment that enters the basin at its southeast tip, to the Jordan segment, exiting the basin at its northwest tip (Garfunkel, 1981). The basin is bounded on both sides by the continuation of the strike–slip faults (Ben-Avraham and Ten Brink, 1989; Garfunkel and Ben-Avraham, 1996), but the actual extension of these segments is not well known. At its southern end, the basin is closed by a series of normal faults, the most visible being the Amazyahu fault, oriented NW–SE, which exhibits at least 50 m of downdip displacement, with a pronounced sub-surface continuation (Kashai and Crocker, 1987; Ben-Avraham, 1997; Al-Zoubi et al., 2002). At the northern extremity of the basin, no normal fault has ever been evidenced (Garfunkel, 1981), while normal faulting is largely present lengthwise the Dead Sea basin, dissecting small quaternary alluvial fans along the coast (Gardosh et al., 1990). A network of faults, parallel to the main direction of the DSF (~20°N) has been described on the western flank of the basin that could possibly be activated during strike–slip motion (Reches and Hoexter, 1981; Gilat, 1991; Garfunkel and Ben-Avraham, 1996).

North of the Dead Sea basin, the fault system is partly concealed by Pleistocene to recent sediments (Fig. 1). The Jericho fault cuts across and along the Jordan valley up to the Sea of Galilee (Ben-Menahem et al., 1976; Garfunkel, 1981; Al-Zoubi et al., 2002). Its morphology is quite similar to the southern part of the fault in the Arava Valley, namely, linear segments separated by small jogs, either compressive or extensive (Ben-Avraham et al., 1996). The Sea of Galilee, as the Dead Sea basin, is associated with a large extensive jog, the components of which are not yet mapped in detail. In addition to the main fault, the Carmel–Gilboa fault, which is branching out from the Dead Sea fault system, is formed by a normal-like prominent fault scarp connected to the Dead Sea fault about 40 km north of the Dead Sea and runs to the Mediterranean sea toward the Cyprian arc (Fig. 1).

Table 1
Origin time, magnitude, location, and focal parameters of the 78 events that satisfy both location and polarity tests

Number	Date and time (yr/mo/day/hr/min/sec)	Magnitude	Latitude °N	Longitude °E	Strike	Dip	Slip
1	87/02/12/22/03/33.63	2.0	32.44	35.25	169.1	84.3	−23.5
2	87/04/29/10/21/55.72	2.4	32.06	35.57	255.8	83.9	177.1
3	88/05/06/04/45/30.97	2.2	32.85	35.64	317.5	88.1	57.4
4	88/05/14/00/35/18.09	2.8	33.21	35.59	87.4	71.5	−130.9
5	88/05/25/01/46/25.80	1.8	31.97	35.38	238.1	80.7	−171.6
6	88/09/02/13/57/45.05	2.5	32.13	35.30	225.6	83.3	171.8
7	88/09/05/14/33/29.09	3.5	33.11	34.51	269.9	19.6	−106.3
8	89/01/03/17/10/46.85	3.9	32.45	35.48	272.6	34.4	−110.4
9	89/01/06/10/59/21.28	3.7	32.45	35.48	290.6	31.5	−100.4
10	90/12/07/20/24/40.59	3.1	32.47	35.30	83.3	59.8	−122.2
11	91/03/01/07/51/52.43	3.3	32.75	35.14	62.3	65.5	−113.9
12	92/04/27/17/24/11.76	2.0	33.01	35.64	320.6	83.9	−50.8
13	92/06/21/07/49/55.19	2.9	32.82	35.21	302.6	80.0	−136.4
14	92/07/29/05/30/46.95	3.4	32.35	35.49	338.6	82.4	−26.5
15	92/09/06/10/29/47.87	3.5	33.34	35.49	151.9	89.3	−19.8
16	92/11/06/16/21/53.72	1.9	32.77	35.31	248.6	55.5	−125.1
17	93/01/14/22/58/16.90	1.1	32.83	35.62	271.2	66.6	−137.3
18	93/03/26/06/57/40.67	3.1	32.16	35.26	152.4	90.0	−15.3
19	94/01/26/18/21/44.18	2.2	32.61	35.61	345.6	76.9	−37.4
20	94/05/30/21/58/44.78	2.7	32.81	35.94	315.0	86.6	−157.8
21	94/06/04/00/10/05.83	1.5	32.98	35.40	241.1	69.6	−138.8
22	94/07/13/04/10/52.20	1.7	32.63	35.12	65.4	48.8	−109.4
23	94/09/16/03/18/57.02	4.1	32.04	35.47	100.4	87.3	−154.2
24	95/08/08/00/15/51.94	3.5	32.41	35.55	273.5	81.6	−172.4
25	95/08/12/22/24/40.98	2.6	32.79	35.63	251.2	87.7	165.1
26	95/11/08/21/40/57.33	2.7	32.09	35.27	59.9	58.3	−106.8
27	96/01/01/21/50/57.83	2.0	32.88	35.63	110.8	79.0	−130.2
28	87/01/01/18/07/23.72	2.4	31.26	35.40	6.0	84.9	−15.2
29	87/04/03/10/59/09.99	2.0	31.28	35.35	117.5	86.9	−142.4
30	87/04/19/06/14/16.58	3.1	31.08	35.50	100.9	81.4	−140.8
31	87/04/22/08/26/48.27	2.6	31.08	35.44	6.2	88.4	−6.5
32	87/05/08/23/09/37.19	3.3	31.09	35.49	5.0	86.9	−10.1
33	87/06/06/20/50/03.20	2.7	31.24	35.37	5.3	83.0	−19.7
34	87/08/15/05/24/47.41	2.5	31.08	35.50	359.4	84.0	−16.7
35	88/01/01/19/36/35.83	3.0	31.15	35.40	17.2	72.8	−39.7
36	88/04/01/00/43/58.83	2.4	31.29	35.46	257.3	71.0	−149.4
37	92/01/11/03/46/31.06	3.7	31.24	35.39	12.6	69.0	−42.6
38	92/01/14/01/30/03.29	2.0	31.07	35.47	282.6	76.2	−150.7
39	92/01/21/03/44/36.03	2.0	31.24	35.41	105.2	56.6	−115.2
40	92/06/26/16/41/33.81	3.1	31.07	35.49	347.6	0.7	−18.4
41	92/06/26/17/17/44.09	3.2	31.07	35.50	13.7	84.4	−18.7
42	92/08/22/22/04/40.50	1.6	31.09	35.49	209.0	77.0	−32.7
43	92/10/08/05/17/51.19	2.6	31.30	35.42	7.4	80.7	−24.8
44	92/11/28/01/49/07.58	2.5	31.31	35.43	296.6	84.0	−169.7
45	93/05/28/03/22/46.59	2.9	31.09	35.45	289.0	83.5	−172.6
46	93/08/02/09/12/56.19	4.1	31.50	35.52	244.0	76.1	−158.4
47	93/11/05/22/06/47.76	1.4	31.08	35.38	191.8	85.6	−8.1
48	94/07/11/13/31/51.78	3.0	31.66	35.49	7.5	84.9	−15.7
49	94/08/24/00/35/06.75	1.5	31.08	35.45	18.6	84.9	−19.8
50	95/03/27/23/56/20.39	1.7	31.52	35.54	46.4	8.4	−15.0
51	95/03/28/01/55/40.90	1.5	31.51	35.51	178.8	69.0	−50.8
52	95/08/25/05/25/05.36	3.2	31.33	35.43	296.9	84.3	−171.2
53	95/08/25/05/48/51.41	2.8	31.33	35.43	285.2	80.5	−163.1
54	95/10/27/00/01/53.07	2.1	31.17	35.53	82.5	85.1	−151.0
55	87/08/01/23/40/49.07	3.3	30.55	35.26	148.8	27.3	−91.7
56	88/02/06/05/04/00.05	2.8	30.51	35.18	315.8	86.8	151.6
57	88/02/09/00/49/49.65	3.4	30.53	35.18	25.5	74.0	−43.8
58	88/02/26/12/22/22.32	2.7	30.53	35.18	147.1	10.7	−109.4

Table 1 (*continued*)

Number	Date and time (yr/mo/day/hr/min/sec)	Magnitude	Latitude °N	Longitude °E	Strike	Dip	Slip
59	88/09/03/09/24/50.01	2.1	30.55	35.29	196.7	40.3	−74.6
60	88/09/03/09/40/08.13	2.0	30.56	35.27	194.3	36.2	−76.5
61	88/09/03/16/37/06.84	1.7	30.56	35.26	203.7	48.9	−72.1
62	88/09/03/20/22/18.01	1.7	30.55	35.25	30.6	69.0	−54.1
63	88/10/05/04/07/57.45	3.2	30.39	34.27	95.4	37.2	−114.3
64	88/10/20/12/28/04.81	3.0	30.55	35.29	26.9	55.9	−56.9
65	89/02/16/14/16/27.58	2.3	30.54	35.31	48.3	30.1	−78.6
66	89/03/29/18/14/59.05	3.5	30.31	35.05	347.3	82.0	−23.5
67	89/04/02/16/01/21.80	2.1	30.32	34.98	259.0	81.3	−175.1
68	89/05/23/04/31/59.48	3.3	30.54	35.22	234.6	64.2	−119.3
69	89/05/23/05/42/16.89	3.1	30.52	35.26	65.7	35.1	−106.0
70	89/06/05/19/54/53.32	1.7	30.54	35.23	239.3	55.3	−118.2
71	89/06/13/17/12/04.69	2.5	30.52	35.25	68.9	31.5	−108.2
72	90/07/25/19/28/09.84	3.4	30.70	35.27	210.0	86.0	1.5
73	92/07/15/01/58/32.96	2.2	30.77	35.29	234.0	79.4	−159.0
74	92/10/07/21/41/14.27	3.6	30.49	35.33	207.0	89.7	12.0
75	93/03/29/04/47/21.73	2.3	30.62	35.34	196.7	77.7	−28.0
76	93/12/02/06/49/52.26	2.5	30.78	35.27	251.9	78.3	−167.2
77	94/11/01/06/07/55.99	2.9	29.81	35.01	105.2	89.9	−160.9
78	95/01/02/03/21/24.73	2.4	30.53	35.30	196.1	33.3	−78.7

The numbering refers to Fig. 3. The focal parameters for each event have been determined conjointly to the stress tensor of Fig. 2b in the global inversion. The table is divided into three parts: north of the Dead Sea basin (first subset of 27 earthquakes), Dead Sea basin (second subset of 27 earthquakes), and south of the Dead Sea basin (last subset of 24 earthquakes).

Post-Pliocene vertical displacement along this structure reaches 600 m, while the strike–slip component is not well established, although some observations call for several hundred meters of left-lateral motion (Achmon, 1986). In the region west of the DSF, a fold system inherited from the Syrian Arc Folding Belt (SAFB) is still well developed with numerous secondary features that can be reactivated under the present stress regime (Eyal, 1996). North of the Carmel–Gilboa fault, the tectonic features could have been rotated (Ron et al., 1984) and the structural directions are more complex (Matmon et al., 1999, 2000; Matmon, 2000).

Bartov et al. (2002) summarized the potentially active faults in Israel based on an extensive compilation of geological observations of the above mentioned studies and many others (see references therein). Throughout this study, we compare our results, obtained from seismological observations, with the geological observations, as presented by Bartov et al. (2002). We show that there is a good correlation between both data sets.

3. Data and methods

Since the beginning of the 1980s, the countries bordering the DSF are operating seismological networks, mostly equipped with short-period instruments (Fig. 1). The two principal networks are the Israel Seismic Network (ISN) operated by the Geophysical Institute of Israel (GII; GII catalog, 1983–1996) and the Jordanian Seismological Observatory (JSO), operated by the Natural Resources Authority (NRA; JSO catalog, 1983–1996). The key point of the paper is to use data gathered from the whole set of seismological stations operating in the area.

The data we used were obtained mainly from the Israeli and Jordanian networks, bearing in mind the geographical positions of the stations relative to the DSF (Fig. 1). The stations from other neighboring networks are generally too far from the epicenter of the earthquakes to provide useful information, and thus, only a few data readings of those networks were incorporated in our data set. In order to enrich our data set, however, we included the phase readings from small-aperture temporary networks, which have been operated during different time periods on the territory of Israel. As a whole, 118 stations have been used at least once (Fig. 1), and the overall azimuthal coverage is significantly improved when compared with the coverage of a single national network.

During the compilation of data into a unique set, the synchronization of the clocks between the different networks came as a major issue in some cases. It is possible to retrieve a constant delay or a linear drift between two clocks when several common stations have recorded the same events. These operations, however, introduce some extra uncertainties, and consequently, we did not make use of them. Instead, the data set has

been filtered using the rms for the location of the events (shift between clocks would create irresolvable time delay for the stations of a network) to keep only the data that guarantee the same time for the different networks involved, or unnoticeable differences, and ignoring events with doubtful time determination. The localization of epicenters, using the Hypoinverse algorithm (Klein, 1978), was determined only when the following conditions were fulfilled: at least 10 P-wave phases, several S-wave phases (≥ 2), good azimuthal coverage of stations (maximal opening was less than 90°), and keeping only events with low rms, vertical and horizontal uncertainties. The second step checked the number and the coherency of the polarities. Only the events with at least 10 unambiguous polarities were considered, and the focal mechanisms were determined manually to test and remove earthquakes with noticeable wrong polarities. A total of 407 events fulfilled the location quality test and a subset of 78 events also satisfied the polarity quality test (Table 1).

Several methods have been developed in microtectonics to determine the orientation and the shape of the stress tensor from a population of slickensides. These methods have been extended to focal mechanisms by Gephart and Forsyth (1984) and Rivera and Cisternas (1990), among others. The major advance of the method developed by Rivera and Cisternas (1990) is to use the original data (the onset polarities), the azimuth of the stations and the take-off angles, where the focal mechanisms emerge as a by-product of the inversion. Gephart and Forsyth (1984) needed to use previously determined focal mechanisms, which could introduce some additional uncertainty. In addition, Rivera and Cisternas (1990) method allows to discriminate between the fault plane and the auxiliary plane since the two planes are not symmetrical regarding the stress tensor. Thus, faulting on a given fault plane in a given stress field determines an auxiliary plane, while faulting on this auxiliary plane in the same stress field does not determine the original fault plane in the general case.

4. Global inversion

4.1. Seismicity

Fig. 1 presents the spatial distribution of 78 events with a reliable location. The seismicity concentrates along the main structures previously mentioned. The fault along the Arava Valley exhibits a pronounced morphological signature (Garfunkel et al., 1981; Klinger et al., 2000b), while surprisingly, the seismic activity is quite low. Although the density of stations in this area is rather low compared to the northern areas, any event with magnitude greater than 2.0 is detected and properly located (GII catalog, 1983–1996; JSO catalog, 1983–1996). Thus, the low seismicity observed is not the result of a scarcity of stations but, more probably, reflects the seismological behavior of the fault. The seismic activity near the middle of the Arava segment, about 5 km west of the fault, is not quite well understood. It could be related to the interaction between the DSF system and the older central Sinai shear zone (Bartov, 1974; Moustafa and Khalil, 1994).

A large part of the seismic activity concentrates in the Dead Sea basin (Fig. 1; Van Eck and Hofstetter, 1989; Salamon et al., 1996). The asymmetry of the basin (Ten Brink et al., 1993; Dooley and McClay, 1997) is underlined by the seismicity: most of the activity concentrates in the northern basin, along the eastern side. A cluster of events, just north of the Lisan Peninsula, can be associated to an east–west fault, which borders the southern and northern Dead Sea basins (Zak and Freund, 1981). We note that the Amatzyahu normal fault that bounds the southern part of the southern basin has almost no seismic signature, and no geological evidence for this fault to be active recently was gathered yet.

North of the Dead Sea, the tectonics becomes more complex and it is difficult to unambiguously associate each event to a specific fault (Fig. 1). Just north of the Dead Sea, a concentration of events underlines the junction of the Carmel–Gilboa faults with the Jordan valley segment of the DSF (Hofstetter et al., 1996). We note the cluster of activity north of the Sea of Galilee and the prolongation of the activity through the Lebanon Mountains.

4.2. Stress tensor and focal mechanisms

The inversion of the stress tensor is highly nonlinear and, therefore, follows an iterative process. In such nonlinear inverse problems, the solution should closely depend on the initial parameters and, generally, it is rather difficult to estimate the quality of the final solution. The error ellipses associated with the principal directions of the tensor could be considered as an indicator of quality of the solution. However, these ellipses are calculated from the partial derivatives of the covariance matrix and give only local information on the final solution and by no means information on its degree of uniqueness. Information about uniqueness may be obtained from the value of the likelihood function in every point of the space of the solutions. It can be achieved by scanning the whole space of the

initial models. We reduced the size of the problem by performing several thousands of inversions with a priori solutions randomly generated. In the following, we present only one representative complete solution, the stress tensor orientation (Fig. 2) and shape together with the associated focal mechanisms (Fig. 3, Table 1), and the orientation of the best solutions.

The family of 200 possible orientations of the stress tensor with likelihood, normalized to 1, greater than 0.98 are presented in Fig. 2a, obtained after the inversion of the data set of the 78 events. For illustration purposes, Fig. 2b shows one of the solutions. The solutions (Fig. 2a) show a fair stability of the direction of the minimum principal component of the stress tensor. Whatever the initial solution is, the inversion converges to a direction of σ_3 close to the horizontal, with an azimuth N40±15°. The shape of the stress tensor is stable, which is in this case $R=(\sigma_1-\sigma_3)/(\sigma_2-\sigma_3)$. It is always greater than 1 and frequently even close to 2, values that characterize an extensional regime (Armijo et al., 1982). The directions of σ_1 and σ_2 are more scattered. Most of the solutions fall in a rather narrow range of azimuth, while the range of the dip is wider. However, the dip values of σ_1 are within the range 40–90° and those of σ_2 are within the range 0–30°, with only a very few exceptions. If some rotation of σ_1 and σ_2 is allowed around the direction of σ_3, a complete inversion of the two directions is precluded. The relative indetermination of the orientations of σ_1 and σ_2 is probably due to two principal reasons. The first reason is the obvious limitation due to the number of available data. However, more data are not necessarily the key to this problem if these additional data are only redundant. Locally, the error ellipse will be reduced, but not the non-uniqueness level of the solution. The second reason is due to the fact that maybe the region does not offer a sufficient variety of orientations and dips of pre-existing faults to constrain the problem to a unique solution. Nevertheless, it is important to note that the focal mechanisms corresponding to these different solutions are much more stable than the stress tensor itself and are only weakly affected by the uncertainty of the stress principal directions.

A priori, we would have expected σ_1 to be horizontal as σ_3, corresponding to the strike–slip regime, following the typology of Armijo et al. (1982), and in fact, a large number of focal mechanisms present strike–slip faulting. However, the type of faulting depends on the orientation and the shape of the stress tensor and on the geometry of the pre-existing faults. In our case, many faults are vertical or sub-vertical, so that σ_1 is within the fault plane or very close to it and is, consequently, inhibited. Under this condition, σ_2 acts as σ_1 and the result is strike–slip faulting on the vertical faults striking obliquely to σ_3 and σ_2.

A large number of focal mechanisms show strike–slip faulting, usually considered as left-lateral motion (Fig. 3, Table 1). In this case the nodal plane, the closest plane to the North–South direction, is assumed to be the fault plane. Many of them present a normal component to some degree. This type of focal mechanism can be observed all over the region, along the Arava Valley, within the Dead Sea basin, along the Jordan fault and the Sea of Galilee area, and also in the Carmel–Gilboa region. Thus, a second type of mechanism is largely represented, which results from normal faulting. These mechanisms are particularly abundant in the cluster off the Arava Valley segment, within the Dead Sea basin and in the Carmel–Gilboa region.

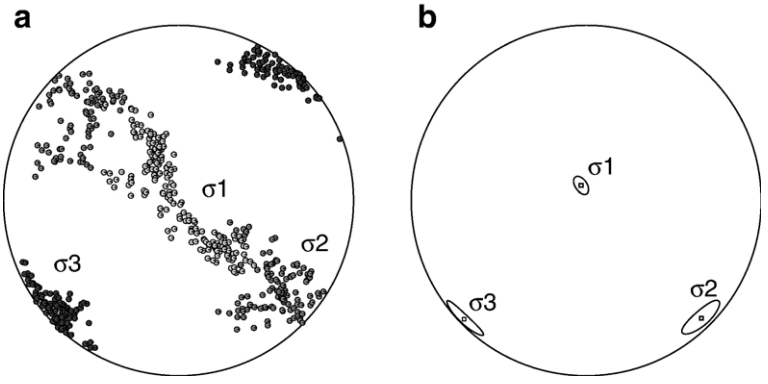

Fig. 2. (a) Example of 200 inversions with randomly generated starting points in the space of initial models. Each of these 200 solutions explains the data with a likelihood value better or equal to 98%. The component σ_3 is very stable; however, σ_1 and σ_2 show stability in azimuth but variation in dip; (b) one of the solutions with error ellipses associated with the principal directions of the stress tensor as determined conjointly based on the 78 focal mechanisms.

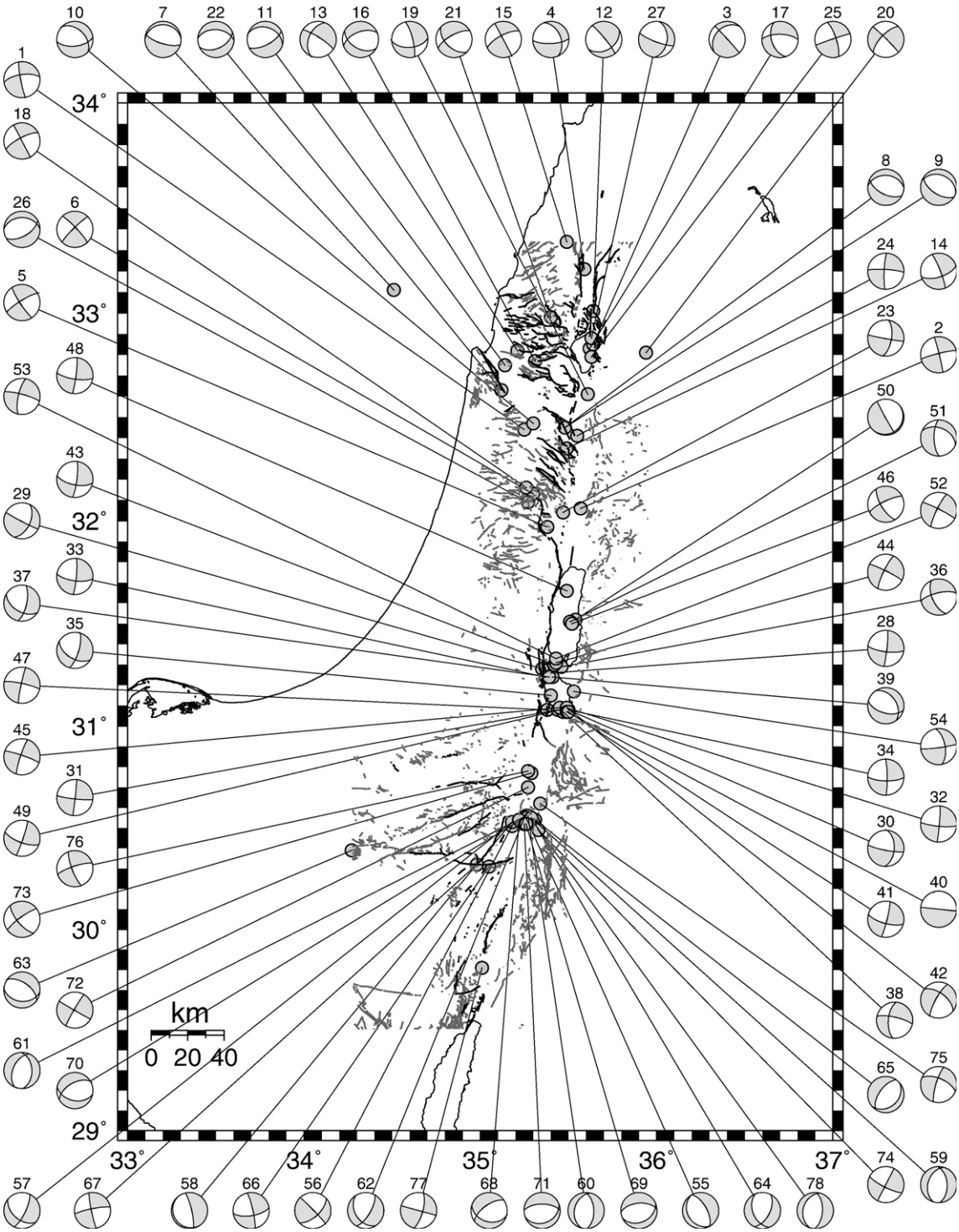

Fig. 3. Focal mechanisms that were derived from the global inversion of the 78 events that satisfy both the location and the polarity tests (see text). The numbering of the focal mechanisms refers to Table 1.

5. Regionalization

In the second step we divided the whole region into three zones on the basis of morphostructural units and many geological and tectonic studies, i.e., Quennell (1958), Freund et al. (1970), Garfunkel (1981), Garfunkel et al. (1981) and Kashai and Crocker (1987) (Fig. 1). The first region encompasses the Jordan Valley segment (north of the Dead Sea basin). The Dead Sea basin forms the second zone. The third region corresponds to the Arava Valley segment (south of the Dead Sea basin), from the Gulf of Aqaba to the Dead Sea basin. In fact, in the third region, there are only a few events along the main fault, and the data for this region are dominated by the data from the cluster at the middle and off the main fault. While the last two regions have a strong internal unity, the first one corresponds to a mixture of tectonically units, dominated by the Carmel–Gilboa system, the Jordan fault and their junction.

5.1. Jordan Valley

Barazangi et al. (1993) speculated that in this region a large part of the structures might be inherited from an ancient tectonic episode that corresponds to the setting of the Palmyrides Range and the Syrian Fold Arc Belt (Krenkel, 1924; Salamon et al., 1996). We selected 27 events in this region. The results of the inversion are shown in Fig. 4 superposed on the potentially active faults (Bartov et al., 2002; and references therein). As for the whole data set, we spanned the space of the initial solutions. The solution presented here (Fig. 5) is only one of the numerous "good" solutions we have obtained. The component σ_3 has the same orientation as in the global inversion. The representative stress tensor (Fig. 5), with σ_1 and σ_3 horizontal and a shape factor, $R=(\sigma_2-\sigma_3)/(\sigma_1-\sigma_3)$ that is equal to 0.5, corresponds to a true strike–slip regime (Armijo et al., 1982). Most of the focal mechanisms indicate strike–slip faulting with a normal component that becomes preponderant in some cases. It is worth noting that the orientation of the principal components of the stress tensor that we obtain in this area are in good agreement with those obtained from a different approach by Ron et al. (1991) and Hofstetter et al. (1996).

The inversion process allows distinguishing which is the actual fault plane between the two nodal planes for 15 focal mechanisms (Fig. 4, Table 2). It is difficult to associate mechanisms 1, 2, 7, 10, 11, 14, 15, 20, 23 and 27 with the exposed faults because either there are no active surface faults or the focal mechanism does not agree with the general strike direction of the fault, while mechanisms 3–6, 8, 9, 12, 13, 16, 18, 19 and 21–26 are in agreement with the strike of the faults mapped from field observations. Event 24 corresponds to a pure strike–slip faulting on a north–south plane and is, obviously, associated with the Jordan fault. For 12 events, the inversion failed to distinguish which plane is the fault plane. For some events, more information is necessary to determine the actual fault plane, while it is relatively straightforward to associate events 4, 8–10, 17, and 22 with known faults (Fig. 4).

5.2. Dead Sea basin

As in the northern area, 27 events were used for the inversion (Fig. 4, Table 2). There are more events in the southern part of the Dead Sea basin and near the Lisan Peninsula (about 20 km northward) than in the northern part of the basin. This is simply due to additional data from the deployment of a temporary network in this area. The stress tensor (Fig. 5) is comparable to that found north of the Dead Sea basin, namely, a strike–slip regime, with σ_1 and σ_3 horizontal and a shape factor equal to 0.4. However, we find that the principal directions are rotated by about 25° clockwise (Fig. 5). The inversion scheme could identify the fault planes in 24 events out of 27 (Fig. 4). It is clear that strike–slip faulting is the dominant feature, whereas normal faulting is expected in a region where the morphology seems to be controlled by the large normal faults, which bound the Dead Sea basin (Garfunkel, 1981; Kashai and Crocker, 1987; Garfunkel and Ben-Avraham, 1996). Several focal mechanisms exhibit a N–S faulting and a left-lateral movement (events 28, 30, 38, 42, 44, 45 and 51–53), in agreement with the results of Van Eck and Hofstetter (1989). The latter underlines the continuity within the southern basin of the strike–slip faulting documented north and south of the Dead Sea basin.

The mechanisms of several events, which are located at the southern tip of the Dead Sea, suggest faulting along east–west direction and, thus, right-lateral movement (events 31, 32, 34, 35, 40, 41, 47 and 49 in Fig. 4). All these events are located at the southern tip of the Dead Sea. Two hypotheses can explain this feature. Based on a study of Ron et al. (1984), Gilat (1991) speculated that the formation of the Dead Sea basin has resulted from the counterclockwise rotation of several microblocks between the left-lateral main faults that bound the basin on each flank. Thus, the counterclockwise rotation means right-lateral movement on a fault striking E–W. Based on field observations, Gilat (1991)

proposed a kinematic model, which shows systematic E–W right-lateral offsets along the flanks of the basin. Another hypothesis comes from the observations of Ben-Avraham and Zoback (1992) and Csato et al. (1997) of large E–W faults, which separate the different basins forming the Dead Sea. In conclusion, the events

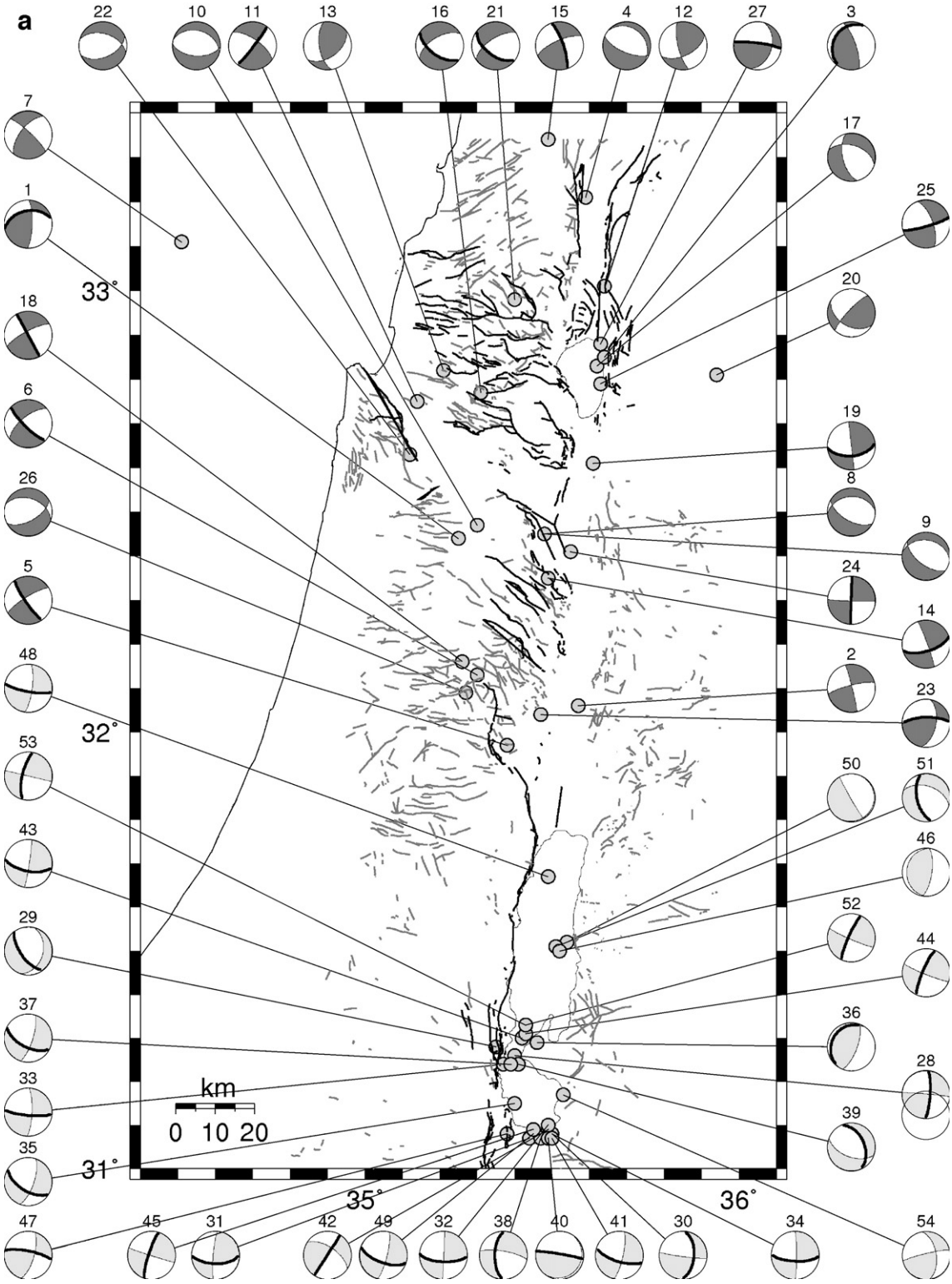

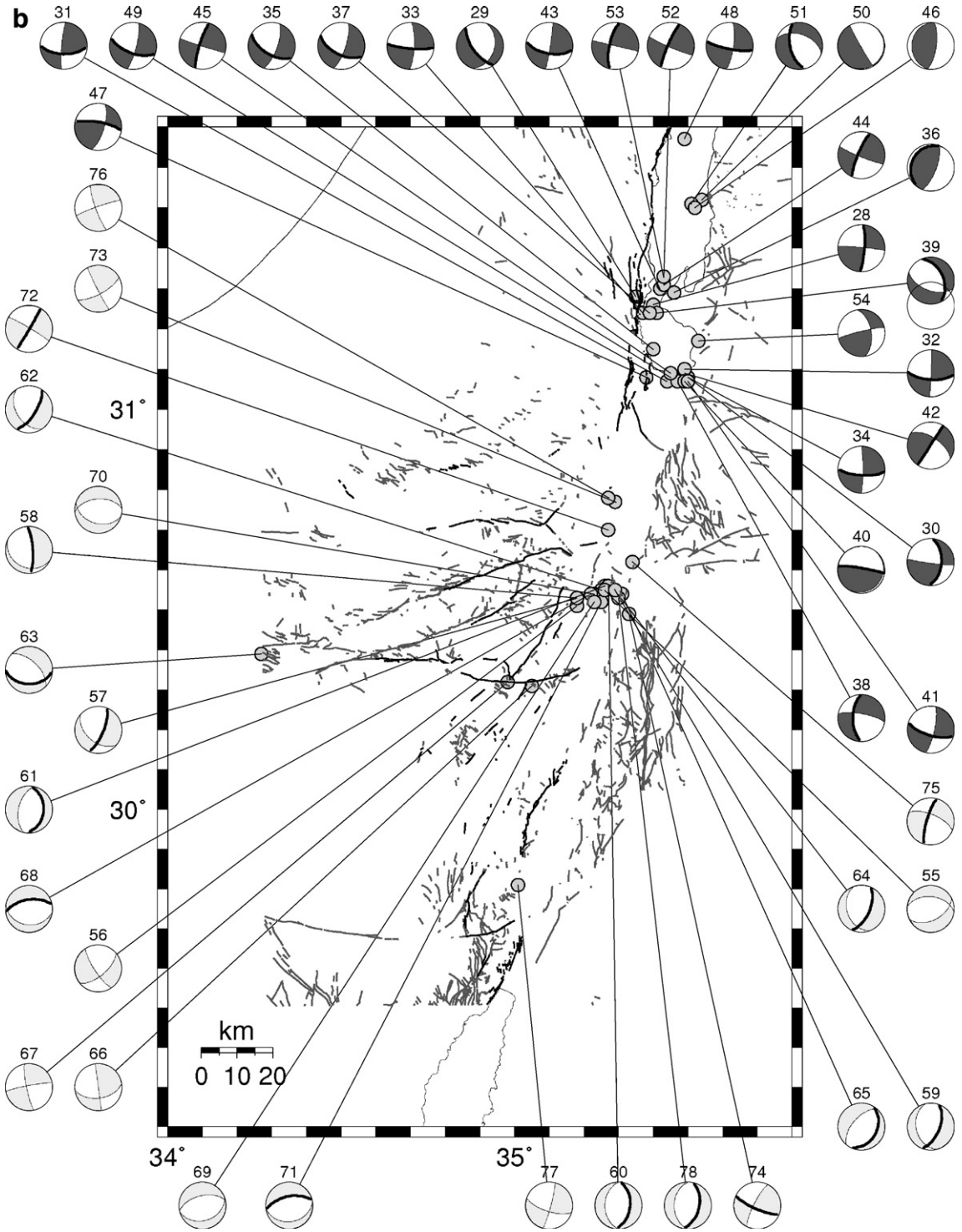

Fig. 4. Regionalization of the inversion results, where parts a and b show north and south of latitude 31°N, respectively, and the activity in the Dead Sea basin is shown in both parts. The three different regions are distinguished by different colors of the focal mechanisms. The thick line in each focal sphere corresponds to the fault plane, when it was possible to discriminate it during the inversion, and the dashed line is the auxiliary plane. Switching of the two planes for a constant stress tensor is not permitted. For a few events, the discrimination between fault plane and auxiliary plane has not been possible (both thin lines). The numbering refers to Table 2, allowing comparison of focal parameters for each event between the global inversion (Table 1) and the regional inversion (Table 2). The grey and black fault lines represent faults (not known to be active) and potentially active faults, respectively (Bartov et al., 2002).

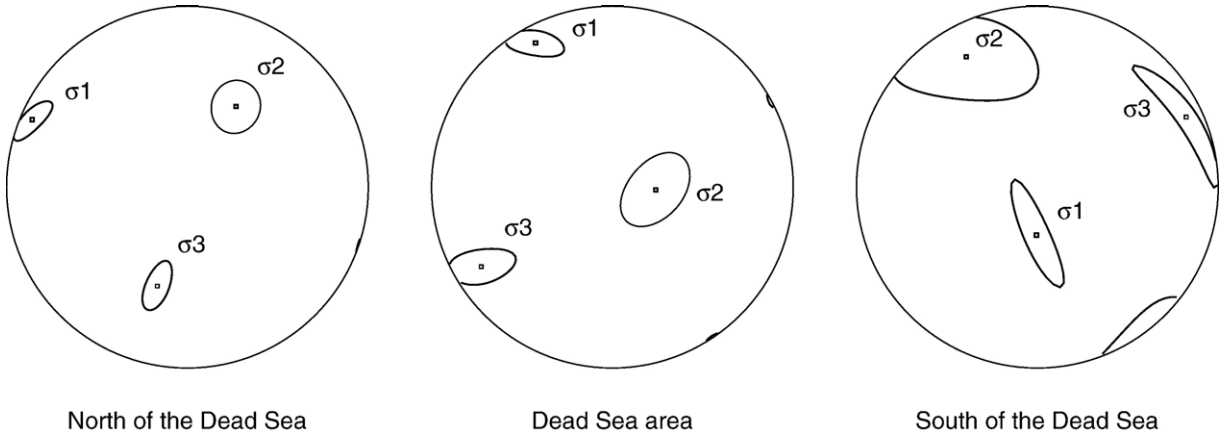

Fig. 5. Representative stress tensor for each region, corresponding to the focal mechanisms of Fig. 4.

we observe reflect widening of the aperture of the basin in a direction normal to its elongation.

There is a pronounced seismic activity in the Lisan Peninsula, which bisects the southern Dead Sea basin from the northern one (events 28, 29, 33, 36, 37, 43, 44, 52, and 53 in Fig. 4). The focal mechanisms are mainly strike slip, with four out of nine being left lateral, three being right-lateral, one being reverse and one being normal faulting. These events are located on a system of left-lateral as well as normal and reverse faults, which were recently mapped by Bartov and Sagy (personal communication). The faulting is in agreement with the results of Van Eck and Hofstetter (1989). The character of faulting in the northern Dead Sea basin is mixed, including right-lateral strike–slip motion along east–west direction and left-lateral strike–slip motion along the Jericho and Arava faults in events 48 and 51, respectively. The faulting in events 46 and 50 suggest a dip–slip motion, probably on a vertical plane in the north–south direction.

5.3. Arava Valley

There are 24 earthquakes in this segment occurring mainly off the main fault. The inversion scheme could identify the fault plane in 16 earthquakes out of 24. The stress tensor is presented in Fig. 5.

Most of the activity (16 events out of 24) is concentrated just north off the junction of the Central Sinai shear zone or Paran fault, Zofar fault, and the Dead Sea fault (see Fig. 4 and Table 2). The geological system associated with the junction of the Central Sinai shear zone and the Dead Sea fault is rather complex (Fig. 4). There are three main faults, forming a triangle, on which we observe the seismic activity, the Dead Sea fault, Paran fault, and the Barak fault. The Paran fault is actually the continuation of the Central Sinai shear zone (Bartov, 1974). These events are clearly associated with the active faults (Bartov et al., 2002) or with subsurface faults (Frieslander et al., 1997; Frieslander, 2000).

The focal mechanisms along the Paran fault are mainly strike–slip faulting striking in the east–west direction (events 66, 67 in Fig. 4 and Table 2). We could not identify the fault planes in these earthquakes; however, we prefer the plane that strikes in the east–west direction, parallel to the Paran fault and, thus, suggesting a right-lateral motion (Bartov, 1974; Dvory, 2002).

The focal mechanisms along the Zofar fault are mixed and include left-lateral strike–slip motion in events 56–58, and normal faulting in events 59–62 and 64. In event 56, we could not determine the preferred fault plane. We surmise that based on the geological lineation of the Zofar fault, inferred from observations of young activity (Bartov et al., 1998; Avni, 2000), the preferred fault plane strikes in the northeast–southwest direction, and all the faults planes dip eastward or ESE.

In event 74, located in the W. Arava, we determine a right-lateral strike–slip motion. In events 68 and 71, we determine a normal mechanism and the fault planes dip northward at angles of almost 60°. The focal mechanisms of events 55, 69 and 70 are similar but the fault planes cannot be determined. The mechanisms of the above mentioned events probably suggest a fault that transverses the Arava valley (Frieslander et al., 1997; Frieslander, 2000).

The focal mechanisms along the Arava–Dead Sea fault are mixed and include strike–slip motion (events 75 and 77) and the dip of the fault plane is rather steep and normal faulting (events 65, and 78), where the fault planes dip eastward. In event 77, we could not define the fault plane; however, based on the geological evidence, we prefer the left-lateral strike–slip motion.

Table 2

Number	Date and time (yr/mo/day/hr/min/sec)	Magnitude	Latitude °N	Longitude °E	Strike	Dip	Slip	Fault name	Fit
1	87/02/12/22/03/33.63	2.0	32.44	35.25	**257.3**	**45.3**	**159.9**	*Faria*	y
2	87/04/29/10/21/55.72	2.4	32.06	35.57	346.2	86.8	10.3	*Jericho*	*y*
3	88/05/06/04/45/30.97	2.2	32.85	35.64	**213.8**	**25.1**	**140.1**	Sheikh Ali	**y**
4	88/05/14/00/35/18.09	2.8	33.21	35.59	113.0	66.8	−97.4	Tel Hay	**y**
5	88/05/25/01/46/25.80	1.8	31.97	35.38	**146.1**	**80.5**	**−12.5**	Samia	**y**
6	88/09/02/13/57/45.05	2.5	32.13	35.30	**134.9**	**76.6**	**−25.4**	Samia	**y**
7	88/09/05/14/33/29.09	3.5	33.11	34.51	313.0	80.3	28.0	Carmel?	y
8	89/01/03/17/10/46.85	3.9	32.45	35.48	119.5	59.1	−71.7	Revaya	y
9	89/01/06/10/59/21.28	3.7	32.45	35.48	280.7	33.0	−112.9	Revaya	y
10	90/12/07/20/24/40.59	3.1	32.47	35.30	286.5	36.1	−79.3	*Faria*	y
11	91/03/01/07/51/52.43	3.3	32.75	35.14	**37.0**	**85.2**	**−157.4**	*Ibtin*	**n**
12	92/04/27/17/24/11.76	2.0	33.01	35.64	64.0	55.9	159.1	Hula	*y*
13	92/06/21/07/49/55.19	2.9	32.82	35.21	170.6	61.2	46.4	Atzmon	n
14	92/07/29/05/30/46.95	3.4	32.35	35.49	**71.8**	**65.0**	**−175.4**	*Mehola*	n
15	92/09/06/10/29/47.87	3.5	33.34	35.49	**340.5**	**76.6**	**19.1**	Roum	**y**
16	92/11/06/16/21/53.72	1.9	32.77	35.31	**126.0**	**56.3**	**−37.6**	Bet Rimon	**y**
17	93/01/14/22/58/16.90	1.1	32.83	35.62	286.9	47.7	−138.7	Ein Gev	*y*
18	93/03/26/06/57/40.67	3.1	32.16	35.26	**151.9**	**89.8**	**−13.5**	*Samia*	**y**
19	94/01/26/18/21/44.18	2.2	32.61	35.61	**83.8**	**53.6**	**−179.2**	*Tel Kazir*	**n**
20	94/05/30/21/58/44.78	2.7	32.81	35.94	120.8	43.0	163.4	N/A	
21	94/06/04/00/10/05.83	1.5	32.98	35.40	**126.9**	**55.1**	**−31.9**	*Meron*	**y**
22	94/07/13/04/10/52.20	1.7	32.63	35.12	286.9	47.7	−60.0	Carmel	*y*
23	94/09/16/03/18/57.02	4.1	32.04	35.47	**268.3**	**71.9**	**143.9**	*Jordan Valley*	**n**
24	95/08/08/00/15/51.94	3.5	32.41	35.55	**1.8**	**89.9**	**−3.3**	Gilboa	**y**
25	95/08/12/22/24/40.98	2.6	32.79	35.63	**74.0**	**81.2**	**−156.2**	*Ein Gev*	**n**
26	95/11/08/21/40/57.33	2.7	32.09	35.27	289.1	42.0	−50.2	*Samia*	*y*
27	96/01/01/21/50/57.83	2.0	32.88	35.63	**277.8**	**82.3**	**130.6**	*Jordan*	**n**
28	87/01/01/18/07/23.72	2.4	31.26	35.40	**5.3**	**79.9**	**3.0**	Lisan	**y**
29	87/04/03/10/59/09.99	2.0	31.28	35.35	**144.7**	**64.5**	**−118.2**	Lisan	**y**
30	87/04/19/06/14/16.58	3.1	31.08	35.50	**4.0**	**51.8**	**−5.6**	DS East. border	**y**
31	87/04/22/08/26/48.27	2.6	31.07	35.44	**91.0**	**61.2**	**171.9**	DS East. border	**y**
32	87/05/08/23/09/37.19	3.3	31.10	35.49	**93.1**	**67.4**	**−178.4**	DS East. border	**y**
33	87/06/06/20/50/03.20	2.7	31.24	35.37	**94.9**	**79.9**	**−166.5**	Lisan	**y**
34	87/08/15/05/24/47.41	2.5	31.08	35.50	**91.6**	**72.0**	**−174.6**	Lisan?	**y**
35	88/01/01/19/36/35.83	3.0	31.15	35.40	**121.4**	**59.6**	**−157.1**	Ein Bokek	**y**
36	88/04/01/00/43/58.83	2.4	31.29	35.46	**212.8**	**19.7**	**101.3**	Lisan	**y**
37	92/01/11/03/46/31.06	3.7	31.24	35.39	**117.6**	**59.3**	**−161.5**	Mor	**y**
38	92/01/14/01/30/03.29	2.0	31.07	35.47	**181.9**	**60.9**	**−16.6**	W. Araba	**y**
39	92/01/21/03/44/36.03	2.0	31.24	35.41	**335.6**	**44.5**	**−54.7**	Lisan	**n**
40	92/06/26/16/41/33.81	3.1	31.07	35.49	**38.5**	**9.1**	**28.9**	W. Araba	**y**
41	92/06/26/17/17/44.09	3.2	31.07	35.50	**107.2**	**69.8**	**−166.4**	W. Araba	**y**
42	92/08/22/22/04/40.50	1.6	31.09	35.49	**303.6**	**60.9**	**−179.3**	W. Araba	**y**
43	92/10/08/05/17/51.19	2.6	31.30	35.42	**100.7**	**62.9**	**−175.7**	Lisan	**y**
44	92/11/28/01/49/07.58	2.5	31.31	35.43	**203.1**	**79.0**	**6.1**	Lisan	**y**
45	93/05/28/03/22/46.59	2.9	31.09	35.45	**197.8**	**80.6**	**1.5**	W. Araba	**y**
46	93/08/02/09/12/56.19	4.1	31.50	35.52	183.8	19.6	85.7	W. Araba	*y*
47	93/11/05/22/06/47.76	1.4	31.08	35.38	**281.1**	**75.5**	**159.1**	Mt. Sodom	**y**
48	94/07/11/13/31/51.78	3.0	31.67	35.49	**100.7**	**77.9**	**−165.9**	Jericho	**y**
49	94/08/24/00/35/06.75	1.5	31.08	35.45	**109.7**	**64.9**	**−166.7**	W. Araba	**y**
50	95/03/27/23/56/20.39	1.7	31.52	35.54	150.2	87.2	−94.0	W. Araba?	*y*
51	95/03/28/01/55/40.90	1.5	31.51	35.51	**167.2**	**59.4**	**−49.8**	W. Araba?	**y**
52	95/08/25/05/25/05.36	3.2	31.33	35.43	**204.1**	**81.6**	**5.5**	Lisan	**y**
53	95/08/25/05/48/51.41	2.8	31.33	35.43	**192.9**	**70.9**	**−1.0**	Lisan	**y**
54	95/10/27/00/01/53.07	2.1	31.17	35.53	256.5	83.8	144.9	DS East. border	*y*
55	87/08/01/23/40/49.07	3.3	30.55	35.26	62.4	49.2	−114.0	Zofar	*y*
56	88/02/06/05/04/00.05	2.8	30.51	35.18	146.3	76.5	−153.2	Zofar	*y*
57	88/02/09/00/49/49.65	3.4	30.53	35.18	**22.2**	**71.4**	**−46.5**	Zofar	**y**
58	88/02/26/12/22/22.32	2.7	30.53	35.18	**355.8**	**77.1**	**−68.6**	Zofar	**y**

(continued on next page)

Table 2 (*continued*)

Number	Date and time (yr/mo/day/hr/min/sec)	Magnitude	Latitude °N	Longitude °E	Strike	Dip	Slip	Fault name	Fit
59	88/09/03/09/24/50.01	2.1	30.55	35.29	**21.6**	**58.5**	**−69.5**	W. Araba	**y**
60	88/09/03/09/40/08.13	2.0	30.56	35.27	**4.4**	**49.0**	**−87.5**	W. Araba	**y**
61	88/09/03/16/37/06.84	1.7	30.56	35.26	**3.4**	**36.8**	**−97.7**	W. Araba	**y**
62	88/09/03/20/22/18.01	1.7	30.55	35.25	**31.9**	**66.9**	**−49.6**	Zofar	**y**
63	88/10/05/04/07/57.45	3.2	30.39	34.27	**89.6**	**41.1**	**−126.1**	Paran	**y**
64	88/10/20/12/28/04.81	3.0	30.55	35.29	**24.3**	**61.0**	**−64.5**	W. Araba	**y**
65	89/02/16/14/16/27.58	2.3	30.54	35.31	**28.9**	**32.3**	**−100.4**	W. Araba	**y**
66	89/03/29/18/14/59.05	3.5	30.31	35.05	172.3	89.8	39.1	Paran	*y*
67	89/04/02/16/01/21.80	2.1	30.32	34.98	168.5	81.6	−5.9	Paran	*y*
68	89/05/23/04/31/59.48	3.3	30.54	35.22	**260.9**	**59.2**	**−99.1**	Zofar	**y**
69	89/05/23/05/42/16.89	3.1	30.52	35.23	256.4	55.3	−88.0	Zofar	y
70	89/06/05/19/54/53.32	1.7	30.54	35.23	265.7	51.1	−103.7	W. Araba	*y*
71	89/06/13/17/12/04.69	2.5	30.52	35.25	**257.5**	**59.4**	**−92.8**	Aqaba–Gharandal	**y**
72	90/07/25/19/28/09.84	3.4	30.70	35.27	**30.8**	**87.6**	**3.8**	Sheizaf	**y**
73	92/07/15/01/58/32.96	2.2	30.77	35.29	61.4	71.0	175.8	Sheizaf	y
74	92/10/07/21/41/14.27	3.6	30.49	35.33	**113.8**	**76.7**	**167.1**	Aqaba–Gharandal	**n**
75	93/03/29/04/47/21.73	2.3	30.62	35.34	**196.4**	**76.2**	**−25.6**	W. Araba	**y**
76	93/12/02/06/49/52.26	2.5	30.78	35.27	159.9	80.7	−5.3	Sheizaf	y
77	94/11/01/06/07/55.99	2.9	29.81	35.01	107.4	69.1	−173.8	Timna	*y*
78	95/01/02/03/21/24.73	2.4	30.53	35.30	**11.8**	**50.2**	**−82.9**	Aqaba–Gharandal	**y**

The same events as in Table 1 are divided into three main regions. Focal parameters have been determined in the regional inversion and correspond to the stress tensors of Fig. 5. The numbering refers to Fig. 4. Bold strike, dip, and rake represent the preferred fault plane resulting from the inversion. The naming of the surface geological faults (using regular letters) is based on Bartov et al. (2002, and references therein), where italic letters denote a probable sub-surface continuation of the fault. The fit column on the right shows the fit or misfit between the surface geological fault and the fault mechanism, where "**y**" (bold) denotes a good fit (within ±20° of the strike of the surface fault), "y" (regular) means a probable good fit since the geological fault cannot be traced on the surface, "*y*" (italic) denotes that the fit of one of the fault planes is probably good but no fault plane was determined, "**n**" (bold) denotes a misfit between the determined fault plane and the (probable) surface geological fault, and "n" (regular) denotes a misfit between the surface geological fault and the focal mechanism (no fault plane was determined).

There are several earthquakes that occur off the main Dead Sea transform and are not part of the Paran cluster. Events 73 and 76 are located on the extension of the Sheizaf fault (Frieslander, 2000). In those events, we could not define the fault plane; however, based on the geological evidence, we prefer the fault plane to be in the NE–SW to ENE–WSW directions, in agreement with the focal mechanism of event 72, and thus implying a left-lateral strike–slip motion. Event 63 occurred on the western continuation of the Ramon fault (Bartov et al., 2002), presenting normal motion with the fault plane dipping southward.

The best solution for the stress tensor (Fig. 5) suggests that σ_1 is nearly vertical and σ_2 and σ_3 are in the horizontal directions, which are close to the directions obtained when the whole set of data was processed (Fig. 2B). The shape factor is 2, a typical value for an extensional regime. Most of the focal mechanisms, i.e., in the Zofar and Wadi Araba faults show normal faulting, and thus agreeing with the shape factor value. Several normal mechanisms have a fault plane striking N–S but slightly rotated clockwise (events 57, 59–62, 64, 65 and 78 in Fig. 4). In other cases, the fault plane strikes E–W (events 55, 63, 68 and 69–71 in Fig. 4 and Table 2). These two directions correspond to the two preferential directions of the tectonic structures related to Central Sinai shear zone (Bartov, 1974; Powell and Khalil, 1993; Eyal, 1996; Bartov et al., 2002). The seismicity on this system is rather weak now. However, it is possible that some interaction with the Arava Valley fault exists that is responsible to the variety of the fault planes encountered there. Van Eck and Hofstetter (1990) have reported similar observations. Outside the cluster, the mechanisms result from strike–slip faulting (events 66, 67 and 72–77 in Fig. 4 and Table 2), so that the area under extension seems to be limited to the cluster.

6. Conclusions

This study takes advantage of many years of continuous seismic monitoring along the southern part of the DSF. Merging data from different seismic networks in this region, and obtaining a better station distribution, reduced uncertainties in the earthquake location. Moreover, the collection of polarity data from the Jordanian and Israeli network is unique and it has allowed us to provide an original set of focal

mechanisms for the regional microseismicity. The 78 earthquakes that have been processed underline the most active tectonic structures of the area that is the Carmel–Gilboa fault system, Dead Sea transform in general and the Dead Sea basin in particular. Surprisingly, despite a clear morphologic signature in the quaternary sediments, the Arava valley displays only minor background seismicity. Considering the simplicity of the southern part of the DSF (the Arava valley), compared with the northern part of the DSF (Dead Sea basin and Carmel–Gilboa fault system), we may expect a fewer secondary structures to accommodate. We can speculate that taking into consideration the tectonic loading in this area, it may lead to the release of the seismic energy only during large earthquakes, which leaves clear imprint in the quaternary morphology (Bowman, 1995; Marco et al., 1996; Klinger et al., 2000b).

Out of 78 earthquakes that have been processed, we could determine the fault planes in 54. There is a very good agreement between the direction and the fault plane, the type of faulting as determined from focal mechanism and the surface or sub-surface active faults (Bartov et al., 2002). In several cases, the earthquakes are located along the continuation of the faults. The occurrences of the earthquakes suggest a sub-surface continuation of the fault that can be revealed using geophysical methods (Frieslander et al., 1997; Frieslander, 2000).

The inversion of the polarities gave us conjoint access to the regional stress tensor and to the focal mechanism for each of the considered earthquakes. The study has shown that it is possible to determine a unique stress tensor for the region that explains most of the polarities recorded. Some variability has also been found in the global inversion of the data. The azimuth of the stress axis is well constrained, and it is in good agreement with what we had expected from the regional geodynamics. In the Arava valley, however, the Paran cluster of events in the Zofar and Wadi Araba faults, which displays a wide range of azimuth for the fault planes, controls the switching of σ_1 and σ_2 as major horizontal stress direction, as it is clearly shown by the regional inversions. When σ_1 is in the vertical direction, it makes the global stress tensor compatible with some local extension, but due to the steep dip of most of the fault plane, inhibiting the effect of the vertical stress component, it allows to have the region behaving under a stress regime dominated by strike–slip. Hence, the majority of the focal mechanisms we have determined show strike–slip motion with a more or less developed normal component. The discrimination between the two nodal planes to determine the fault plane, during the inversion process, indicates that two directions dominate the fault plane population. The first cluster has an azimuth close to N15°, which corresponds to the overall direction of the DSF. The second cluster is closer to N120°, corresponding to the direction of the Carmel–Gilboa fault system. We note that seismicity in the Dead Sea basin is strongly dominated by strike–slip mechanisms, from which a large part have a fault plane oriented perpendicular to the longest axis of the basin, rather than by normal faulting. It is fully consistent with the pull-apart hypothesis of the Dead Sea basin controlled by strike–slip motion along the DSF.

Acknowledgements

C. Ben-Sasson, L. Feldman, and B. Reich did the initial data processing. D. Kadosh, D. Levi, U. Peled and Y. Schwartz kept the seismic network operating. Discussion and fruitful comments of Dr. Y. Bartov significantly improved the manuscript. This study is supported by the Earth Science Research Administration, Ministry of the National Infrastructure, and IPGP contribution 2182. Figures in this study were prepared using the GMT program (Wessel and Smith, 1991).

References

Achmon, M., 1986. The Carmel border fault. M.Sc. Thesis, The Hebrew Univ., Jerusalem, Israel, 102 pp.

Al-Zoubi, A., Shulman, H., Ben-Avraham, Z., 2002. Seismic reflection profiles across the southern Dead Sea basin. Tectonophysics 346, 61–69.

Aldersons, F., Ben-Avraham, Z., Hofstetter, A., Kissling, E., Al-Yazjeen, T., 2003. Lower-crustal strength under the Dead Sea basin from local earthquake and rheological modeling. Earth Planet. Sci. Lett. 214, 129–142.

Amiran, D., Arieh, E., Turcotte, T., 1994. Earthquakes in Israel and adjacent areas: macroseismic observations since 100 B.C.E. Isr. Explor. J. 23, 261–296.

Armijo, R., Carey, E., Cisternas, A., 1982. The inverse problem in microtectonics and the separation of tectonic phases. Tectonophysics 82, 145–160.

Atallah, M., 1992. Tectonic evolution of northern Wadi Araba, Jordan. Tectonophysics 204, 17–26.

Avni, Y., 2000. Subsurface Study of the Paran and Thamad Faults Area. The Hebrew Univ, Jerusalem. 89 pp.

Badawy, A., Horváth, F., 1999. Recent stress field of the Sinai subplate region. Tectonophysics 304, 385–403.

Baer, G., Sandwell, D., Williams, S., Bock, Y., Shamir, G., 1999. Coseismic deformation associated with the November 1995, Mw=7.1 Nuweiba earthquake, Gulf of Elat (Aqaba), detected by synthetic aperture radar interferometry. J. Geophys. Res. 104, 25221–25232.

Barazangi, M., Seber, D., Chaimov, T., Best, J., Sawaf, T., 1993. Tectonic evolution of the northern Arabian plate in western Syria.

In: Boschi, et al. (Ed.), Recent Evolution and Seismicity of the Mediterranean Region. Kluwer Acad. Publish., The Netherlands, pp. 117–140.

Barjous, M., Mikbel, Sh., 1990. Tectonic evolution of the Gulf of Aqaba–Dead Sea transform fault system. Tectonophysics 180, 49–59.

Bartov, Y., 1974. A structural and palegeographical study of the central Sinai faults and domes, Ph.D. thesis, The Hebrew University of Jerusalem.

Bartov, Y., Steinitz, G., Eyal, M., Eyal, Y., 1980. Sinistral movement along the Gulf of Aqaba—its age and relation to the opening of the Read Sea. Nature 285, 220–221.

Bartov, Y., Avni, Y., Calvo, R., Frieslander, U., 1998. The Zofar fault —a major intra-rift feature in the Arava rift valley. Isr. Geol. Surv., Current Res. 11, 27–32.

Bartov, Y., Sneh, A., Fleischer, L., Arad, V., Rosensaft, M., 2002. Potentially active faults in Israel. Geol. Surv. Isr. Rept. 29/2002. 8 pp.

Ben-Avraham, Z., 1985. Structural framework of the Gulf of Elat (Aqaba), northern Red Sea. J. Geophys. Res. 90, 703–726.

Ben-Avraham, Z., 1997. Geophysical framework of the Dead Sea: structure and tectonics. In: Niemi, et al. (Ed.), The Dead Sea: The Lake and Its Setting. Oxford Univ. Press. 22–35 pp.

Ben-Avraham, Z., Ten Brink, U., 1989. Transverse faults and segmentation of basins within the Dead Sea rift. J. Afr. Earth Sci. 8, 603–616.

Ben-Avraham, Z., Zoback, M.D., 1992. Transform-normal extension and asymmetric basins: an alternative to pull-apart models. Geology 20, 423–426.

Ben-Avraham, Z., Ten Brink, U., Bell, R., Reznikov, M., 1996. Gravity field over the Sea of Galilee: evidence for a composite basin along a transform fault. J. Geophys. Res. 101, 533–544.

Ben-Menahem, A., Vered, M., Nur, A., 1976. Tectonics, seismicity and structure of the Afro-Euroasian junction—the breaking of an incoherent plate. Phys. Earth Planet. Inter. 12, 1–50.

Bowman, D., 1995. Active surface ruptures on the northern Arava fault, the Dead Sea Rift. Isr. J. Earth-Sci. 44, 51–59.

Csato, I., Kendall, C., Nairn, A., Baum, G., 1997. Sequence stratigraphic interpretations in the southern Dead Sea basin, Israel. Geol. Soc. Amer. Bull. 108, 1485–1501.

Dooley, T., McClay, K., 1997. Analog modeling of pull-apart basins. Amer. Assoc. Petrol. Geol. Bull. 81, 1804–1826.

Dvory, N.Z., 2002. Subsurface study of the Paran and Thamad faults area. M.SC. Thesis, The Hebrew Univ., Jerusalem, 82 p. (in Hebrew with English Abst.).

Eyal, Y., 1996. Stress field fluctuations along the Dead Sea rift since the middle Miocene. Tectonics 15, 157–170.

Eyal, M., Eyal, Y., Bartov, Y., Steinitz, G., 1981. The tectonic development of the western margin of the Gulf of Elat (Aqaba) rift. Tectonophysics 80, 39–66.

Freund, R., Garfunkel, Z., Zak, I., Goldberg, M., Weissbrod, T., Derin, B., 1970. The shear along the Dead Sea rift. Philos. Trans. R. Soc. Lond. Ser. A: Math. Phys. Sci. 267, 105–127.

Frieslander, U., 2000. The structure of the Dead Sea transform emphasizing the Arava using new geophysical data. Ph.D. Thesis, The Hewbrew Univ., Jerusalem, 101 pp.

Frieslander, U., Bartov, Y., Garfunkel, Z., 1997. The structure of the Arava—new results from geological and geophysical studies. The 13th German–Israel Meeting on the Dead Sea rift, Dead Sea, Israel. Terra Nostra, Schriften der Alfred Wegener Stiftung 4/97.

Gardosh, M., Reches, Z., Garfunkel, Z., 1990. Holocene tectonic deformation along the western margins of the Dead Sea. Tectonophysics 180, 123–137.

Garfunkel, Z., 1981. Internal structure of the Dead Sea leaky transform (rift) in relation to plate kinematics. Tectonophysics 80, 81–108.

Garfunkel, Z., Ben-Avraham, Z., 1996. The structure of the Dead Sea basin. Tectonophysics 266, 155–176.

Garfunkel, Z., Zak, Y., Freund, R., 1981. Active faulting in the Dead Sea rift. Tectonophysics 80, 1–26.

Gephart, J., Forsyth, D., 1984. An improved method for determining the regional stress tensor using focal mechanism data: application to the San Fernando earthquake sequence. J. Geophys. Res. 89, 9305–9320.

GII Seismological Bulletins, 1983–1996. Earthquakes in and around Israel. Seismological Division, Geophysical Institute of Israel.

Gilat, A., 1991. Oversized U-shaped canyon development at the edge of rotating blocks due to wrench faulting on margins of the Dead Sea graben. Terra Nova 3, 638–647.

Ginat, H., Enzel, Y., Avni, Y., 1998. Translocated Plio-Pleistocene drainage systems along the Arava fault of the Dead sea transform. Tectonophysics 284, 151–160.

Hardebeck, J., Hauksson, E., 2001. The crustal stress field in southern California and its implications for fault mechanics. J. Geophys. Res. 106, 21859–21882.

Hauksson, E., 1994. State of stress from focal mechanism before and after the 1992 Landers earthquake sequence. Bull. Seismol. Soc. Am. 84, 917–934.

Hofstetter, A., van Eck, T., Shapira, A., 1996. Seismic activity along the fault branches of the Dead Sea–Jordan transform: the Carmel–Tirtza fault system. Tectonophysics 267, 317–330.

Hofstetter, A., Thio, H.-K., Shamir, G., 2003. Source mechanism of the 22/11/1995 Gulf of Aqaba earthquake and its aftershock sequence. J. Seismol. 7, 99–114.

JSO Seismological Bulletins, 1983–1996. Earthquakes in Jordan and Adjacent Areas. Jordan Seismological Observatory, Amman, Jordan.

Kashai, E., Crocker, P., 1987. Structural geometry and evolution of the Dead Sea–Jordan rift system as deduced from new subsurface data. Tectonophysics 141, 33–60.

Khair, K., 2001. Geomorphology and seismicity of the Roum faultas one of the active branches of the Dead Sea fault system in Lebanon. J. Geophys. Res. 106, 4233–4245.

Klein, R.W., 1978. Hypocenter location program HYPOINVERSE Part I: Users guide to versions 1, 2, 3 and 4. U.S. Geol. Surv. Open-File Report 78–694.

Klinger, Y., Rivera, L., Haessler, H., Maurin, J.-C., 1999. Active faulting in the Gulf of Aqaba: new knowledge from the Mw 7.3 earthquake of 22 November 1995. Bull. Seismol. Soc. Am. 89, 1025–1036.

Klinger, Y., Michel, R., Avouac, J.P., 2000a. Co-seismic deformation during the Mw 7.3 Aqaba earthquake (1995) from ERS-SAR interferometry. Geophys. Res. Lett. 27, 3651–3654.

Klinger, Y., Avouac, J.P., Dorbath, L., Abou Karaki, N., Tisnerat, N., 2000b. Seismic behavior of the Dead Sea fault along Araba valley (Jordan). Geophys. J. Int. 142, 769–782.

Krenkel, E., 1924. Der Syrische bogen. Centralbl. Mineral. Geol. Palaeontol. 9, 274–281.

Le Beon, M., Klinger, Y., Agnon, A., Dorbath, L., Baer, G., Meriaux, A.-S., Ruegg, J.-C., Charade, O., Finkel, R., Ryerson, F., 2006. Geodetic versus geologic slip rate along the Dead Sea fault. Seism Soc. Assoc. Meeting, San Francisco.

Lund, B., Slunga, R., 1999. Stress tensor inversion using detailed microearthquake information and stability constraints: applications to Olfus in southwest Iceland. J. Geophys. Res. 104, 14947–14964.

Marco, S., Stein, M., Agnon, A., Ron, H., 1996. Long term earthquake clustering: a 5000 years paleoseismic record in the Dead Sea graben. J. Geophys. Res. 101, 6179–6191.

Matmon, A., 2000. Landscape analysis as a key to the understanding of the tectonic evolution of the Galilee, northern Israel, during the last 4 million years. Ph.D. Thesis, The Hebrew Univ., Jerusalem, 144 pp.

Matmon, A., Enzel, Y., Zilberman, E., Heimann, A., 1999. Late Pliocene and Pleistocene reversal of drainage system in northern Israel: tectonic implications. Geomorphology 28, 43–59.

Matmon, A., Zilberman, E., Enzel, Y., 2000. Determination of escarpment age using morphologic analysis: an example from the Galilee, northern Israel. Geol. Soc. Amer. Bull. 112, 1864–1876.

Moustafa, A.R., Khalil, M., 1994. Rejuvenation of the Eastern Mediterranean passive continental margin in northern and central Sinai: new data from the Themed fault. Geol. Mag. 131, 435–448.

Pe'eri, S., Wdowinski, S., Shtibelman, A., Bechor, N., Bock, Y., Nikolaidis, R., van Domselaar, M., 2002. Current plate motion across the Dead Sea Fault from three years of continuous GPS monitoring. Geophys. Res. Lett. 29, 1697–1700.

Powell, J.H., Khalil, M., 1993. Structure and sedimentation of Permo-Triassic and Triassic rocks exposed in small-scale horsts and grabens of pre-Cretaceous age: Dead Sea margin, Jordan. J. Afr. Earth Sci. 17, 131–143.

Quennell, A.M., 1958. The structural and geomorphic evolution of the Dead Sea Rift. Quarterly J. Geol. Soc. Lond. 114, 2–24.

Reches, Z., Hoexter, D., 1981. Holocene seismic and tectonic activity in the Dead Sea area: the Dead Sea rift. Tectonophysics 80, 235–254.

Rivera, L., Cisternas, A., 1990. Stress tensor and fault plane solution for a population of earthquakes. Bull. Seismol. Soc. Am. 80, 600–614.

Ron, H., Freund, R., Garfunkel, Z., Nur, A., 1984. Block rotation by strike–slip faulting: structural and paleomagnetic evidence. J. Geophys. Res. 89, 6256–6270.

Ron, H., Nur, A., Hofstetter, A., 1991. Late Cenozoic and recent strike slip tectonics in Mt. Carmel northern Israel. Ann. Tecton. 4, 70–80.

Salamon, A., Hofstetter, A., Garfunkel, Z., Ron, H., 1996. Seismicity of eastern Mediterranean region: perspective of the Sinai subplate. Tectonophysics 263, 293–307.

Sneh, A., 1996. The Dead Sea rift: lateral displacement and downfaulting phases. Tectonophysics 263, 277–292.

Ten Brink, U., Ben-Avraham, Z., Bell, R., Hassouneh, M., Coleman, D., Andersean, G., Tibor, G., Coakley, B., 1993. Structure of the Dead Sea pull-apart basin from gravity analyses. J. Geophys. Res. 98, 21887–21894.

Van Eck, T., Hofstetter, A., 1989. Microearthquake activity in the Dead Sea depression. Geophys. J. Int. 99, 605–620.

Van Eck, T., Hofstetter, A., 1990. Fault geometry and spatial clustering of microearthquakes along the Dead Sea–Jordan fault zone. Tectonophysics 180, 15–27.

Wessel, P., Smith, W., 1991. Free software helps maps and display data. EOS Trans. AGU 72, 441.

Zak, I., Freund, R., 1981. Asymmetry and basin migration in the Dead Sea rift. Tectonophysics 80, 27–38.